GNSS Satellite Fault Detection and Exclusion for Integrated GNSS/INS Systems

Birendra Kujur, Samer Khanafseh, Boris Pervan, *Illinois Institute of Technology*

BIOGRAPHY

Birendra Kujur is currently a PhD candidate in Mechanical and Aerospace Engineering at Illinois Institute of Technology. He received his Bachelor of Science in Mechanical Engineering from Purdue University in 2014. His research interests include multi-sensor navigation systems, navigation integrity monitoring, detecting GNSS spoofing attacks, and developing anti-spoofing solution.

Dr. Samer Khanafseh is currently a research associate professor at Illinois Institute of Technology (IIT), Chicago, and the principal of TruNav LLC. He received his MSc and PhD degrees in Aerospace Engineering from IIT in 2003 and 2008, respectively. Dr. Khanafseh has been involved in several aviation applications such as Autonomous Airborne Refueling (AAR) of unmanned air vehicles, autonomous shipboard landing for NUCAS and JPALS programs and Ground Based Augmentation System (GBAS). His research interests are focused on high accuracy and high integrity navigation algorithms, cycle ambiguity resolution, high integrity applications, fault monitoring and robust estimation techniques. He was the recipient of the 2011 Institute of Navigation Early Achievement Award for his outstanding contributions to the integrity of carrier phase navigation systems.

Dr. Boris Pervan is a Professor of Mechanical and Aerospace Engineering at IIT, where he conducts research on advanced navigation systems. Prior to joining the faculty at IIT, he was a spacecraft mission analyst at Hughes Aircraft Company (now Boeing) and a postdoctoral research associate at Stanford University. Prof. Pervan received his B.S. from the University of Notre Dame, M.S. from the California Institute of Technology, and Ph.D. from Stanford University. He is an Associate Fellow of the AIAA, a Fellow of the Institute of Navigation (ION), and Editor-in-Chief of the ION journal NAVIGATION. He was the recipient of the IIT Sigma Xi Excellence in University Research Award (2011, 2002), Ralph Barnett Mechanical and Aerospace Dept. Outstanding Teaching Award (2009, 2002), Mechanical and Aerospace Dept. Excellence in Research Award (2007), University Excellence in Teaching Award (2005), IEEE Aerospace and Electronic Systems Society M. Barry Carlton Award (1999), RTCA William E. Jackson Award (1996), Guggenheim Fellowship (Caltech 1987), and Albert J. Zahm Prize in Aeronautics (Notre Dame 1986).

ABSTRACT

In this work, we present a Global Navigation Satellite Systems (GNSS) satellite fault detection, identification, and exclusion method for an integrated GNSS/Inertial Navigation System (INS) tightly-coupled navigation architecture. Observed satellite fault profiles and magnitudes are taken as a baseline to design the monitor. Normalized innovations for each satellite are utilized to observe the respective satellite faults on each channel. A sufficient test statistic for each satellite channel is derived using the generalized likelihood ratio test (GLRT). We develop a method for quantifying missed detection rates given fault profile and magnitude. This developed methodology is capable of providing protection levels using the INS-only coasting solution. We also describe an identification and exclusion method using consecutive windows of the monitor without the need for running parallel Kalman filters (KF). We validate the developed algorithm for the detection, identification and exclusion of faulty satellites using simulated fault scenarios.

I. INTRODUCTION

Today, GNSS is widely used for positioning, navigation, and timing (PNT) applications due to its accuracy, continuity, and integrity. Due to its use in safety-critical applications such as aircraft landing, autonomous terrestrial vehicles etc., a threat to GNSS integrity can endanger public safety. Integrity is defined as the probability of a position estimate error exceeding a given alert limit due to undetected faults. The integrity of GNSS systems can be compromised due to undetected satellite faults resulting in inaccurate timing or positioning. Receiver Autonomous Integrity Monitoring (RAIM) was developed as a method to detect GPS satellite faults using the redundancy of multiple satellites (Parkinson and Axelrad (1988), Angus (2006)). This has recently been extended to Advanced Receiver Autonomous Integrity Monitoring (ARAIM), which includes multiple constellations (Blanch et al. (2015)). Over time, auxiliary sensors such as inertial measurement unit (IMU) were also used to aid in satellite fault detection (Brenner (1996)). Modern navigation architectures typically utilize integrated GNSS/INS systems for navigation; hence no additional hardware implementation is required. Also, due to providing better accuracy, continuity,

and protection levels, the integrated GNSS/INS KF architecture is favored over the snapshot positioning methods such as the least-squares solution. Fault detection algorithms such as RAIM and ARAIM typically utilize solution separation between satellite subsets for detection (Blanch et al. (2015)). Solution separation measures the effect of the fault on the position domain (or any specific state(s)) directly. As a result, it does not require defining a specific temporal or spatial fault profile, making the evaluation of the system integrity risk valid for any type of fault without the need to run many simulations to cover all types of faults the system may have. However, RAIM and now ARAIM use snapshot navigation solutions (least squares, for example).

In integrated GNSS/INS systems with KF implementations, however, due to time correlation, it is not sufficient to remove a faulty sensor measurement at the time of detection. This is true because the fault (for example a slowly growing one) may have already corrupted the filter before the test statistic exceeded the detection threshold. Also, to use solution separation parallel sub-filters, one for each fault hypothesis, need operate for detection. Further, to maintain detection capability after exclusion of a fault, it would be necessary to continuously run parallel sub-filters for each sub-filter, thus greatly increasing the computational and memory cost as the number of fault hypotheses increases. Other fault detection methods such as innovation-based detectors (Joerger and Pervan (2013); Tanil et al. (2018)), the Euclidean distance method (Knowles and Gao (2023)) and other different methods Quartararo and Langel (2022); Wendel (2022)) have been proposed. These, like solution separation, are general detection approaches that do not assume any prior knowledge of fault temporal behavior. They avoid the computational burden of KF solution separation approaches, but only at the expense of considerable degradation in detection performance over time.

Table 1 from DO-384 (2020) summarizes the different fault modes, their ranges and fault rates from data on observed faults in GPS satellites from the year 2000 to 2016. Our novel approach to fault detection for an integrated GNSS/INS system aims to first provide a detector for GNSS faults based on the history of observed faults and second reduce the computational cost by detecting and excluding faults on individual satellites using a single KF. In section II we provide a brief background on tightly coupled GNSS/INS and then introduce the satellite fault channel detector. The results of an example detection scenario are shown and discussed in section III. In section IV we detail the identification and exclusion algorithm to be utilized once detection occurs. Section V contains details about the sequential monitor window concept with protection levels. Finally, we summarize the work in section VI. We also provide relevant derivations in the appendices.

Table 1: Summary of assigned fault rates for position testing from Table G-4 in (DO-384 (2020))

Fault mode	**Range**	**Fault Rates** (10^{-5}**/hr/Satellite**)
Ramp	3 cm/s - 1 m/s	10/15
Step	300-700 meters	3/15
Acceleration	0.00005 - 0.025 m/s^2	2/15

II. SATELLITE FAULT CHANNEL DETECTOR

We consider a vehicle employing INS and GNSS sensors integrated using a KF to estimate its position, velocity and attitude. The dynamics of the GNSS/INS system, augmented as needed with sensor error state dynamics, are linearized to obtain the process model utilized in the KF,

$$\mathbf{x}_{k+1} = \mathbf{\Phi}_k \, \mathbf{x}_k + \mathbf{\Gamma}_{w_k} \, \mathbf{w}_k, \tag{1}$$

where $\mathbf{x}_k$ is the state vector, $\mathbf{\Phi}_k$ is the state transition matrix, $\mathbf{\Gamma}_{w_k}$ is the process noise model matrix, and $\mathbf{w}_k$ is the additive white process noise with a respective covariance matrix $\mathbf{Q}_k$. The measurement model is

$$\mathbf{z}_k = \mathbf{H}_k \, \mathbf{x}_k + \boldsymbol{\nu}_k, \tag{2}$$

where $\mathbf{H}_k$ is the observation matrix and $\boldsymbol{\nu}_k$ is the measurement noise with a respective covariance matrix $\mathbf{V}_k$.

The innovation vector $\boldsymbol{\gamma}_k$ with respective covariance matrix $\mathbf{S}_k$ at time epoch k is defined as

$$\boldsymbol{\gamma}_k = \mathbf{z}_k - \mathbf{H}_k \, \bar{\mathbf{x}}_k, \tag{3}$$

where $\bar{\mathbf{x}}$ is the state vector estimate prior to the measurement update at time epoch k. Innovations is the instantaneous difference between GNSS observations and predicted measurement with INS.

At any time k, the normalized fault-free innovation vector $\tilde{\boldsymbol{\gamma}}_k$ of the KF is

$$\tilde{\boldsymbol{\gamma}}_k = \mathbf{S}_k^{-\frac{1}{2}} (\mathbf{z}_k - \mathbf{H}_k \bar{\mathbf{x}}_k), \tag{4}$$

which follows a normal distribution

$$\tilde{\boldsymbol{\gamma}}_k \sim \mathcal{N}(0, \mathbf{I}). \tag{5}$$

We call each element of this vector a satellite innovation channel and a fault appearing in any satellite will appear on its respective channel first. The fault-free normalized innovations of each channel over time are time-independent white Gaussian noise (WGN).

In the faulted scenario the normalized innovation vector at time k is

$$\tilde{\boldsymbol{\gamma}}_k^f = \tilde{\boldsymbol{\gamma}}_k + \mathbf{S}_k^{-\frac{1}{2}}(\bar{\mathbf{f}}_k + \mathbf{b}_k), \tag{6}$$

which follows a normal distribution

$$\tilde{\boldsymbol{\gamma}}_k^f \sim \mathcal{N}(\mathbf{S}_k^{-\frac{1}{2}}(\bar{\mathbf{f}}_k + \mathbf{b}_k), \mathbf{I}), \tag{7}$$

where $\bar{\mathbf{f}}_k$ is the current fault vector, and $\mathbf{b}_k$ is the cumulative effect of prior faults ($\bar{\mathbf{f}}_{1:k-1}$) on the current innovation vector. Note that superscript f is used to denote variables related to faults.

The cumulative term $\mathbf{b}_k$ for $k > 1$ is

$$\mathbf{b}_k = -\mathbf{H}_k \boldsymbol{\Phi}_k [\boldsymbol{\Omega}_{k-1} + \mathbf{K}_{k-1} \boldsymbol{\beta}_{k-1}], \tag{8}$$

where,

$$\boldsymbol{\Omega}_{k-1} = \boldsymbol{\Phi}_{k-1} [\boldsymbol{\Omega}_{k-2} + \mathbf{K}_{k-2} \boldsymbol{\beta}_{k-2}], \tag{9}$$

and

$$\boldsymbol{\beta}_{k-1} = \bar{\mathbf{f}}_{k-1} - \mathbf{H}_{k-1} \boldsymbol{\Omega}_{k-1}, \tag{10}$$

where $\mathbf{K}$ is the Kalman gain. The derivation for this cumulative term is in appendix A.

Using equations (6) through (10), the deterministic effect of current and prior faults on normalized innovations can be obtained. As an example, Figure 1 illustrates the effect of a ramp fault of magnitude 0.1 m/s on the normalized innovations for N epochs. Recall from Table 1 that the ramp fault has been the most observed fault mode.

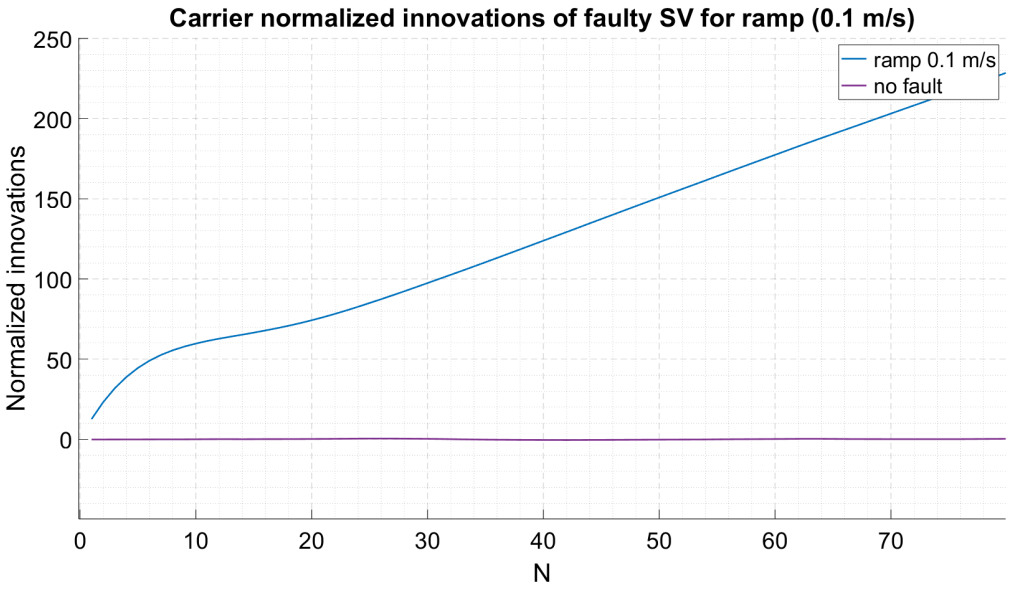

Figure 1: *Example deterministic effect (D) of ramp fault on normalized innovation.*

If we observe the normalized innovations for exposure time N, the deterministic impact ($\mathbf{D}_{1:N}$) of fault on n^{th} satellite is

$${}^n\tilde{\boldsymbol{\gamma}}_{1:N}^f = \mathbf{D}_{1:N} + {}^n\tilde{\boldsymbol{\gamma}}_{1:N} \tag{11}$$

where ${}^n\tilde{\boldsymbol{\gamma}}^f_{1:N}$ is the n^{th} channel normalized innovation time series when a fault is present, and ${}^n\tilde{\boldsymbol{\gamma}}_{1:N}$ is the n^{th} channel normalized innovation time series when no fault is present. As a starting point, we approximate the deterministic impact ($\mathbf{D}_{1:N}$) as a linear ramp,

$$\mathbf{D}_{1:N} \approx \mathbf{M}\theta = [1 \quad 2 \quad 3 \quad . \quad . \quad . \quad N]^T\theta \tag{12}$$

where θ is the unknown magnitude and $\mathbf{M}$ is the ramp subspace vector. Here, θ represents the slope of the ramp.

We formulate the problem as signal detection of unknown amplitude (θ) in WGN (${}^n\tilde{\boldsymbol{\gamma}}_{1:N}$) for each satellite channel. This is a Bayesian linear model ($\mathbf{a} = \mathbf{M}\theta + \mathbf{w}$) detection problem of unknown signal parameter (θ) additive to Gaussian noise ($\mathbf{w}$), with null hypothesis $H_0 : \theta = 0$, and alternative hypothesis $H_1 : \theta \neq 0$. For this type of detection problem where signal parameter and sign are unknown, no uniformly most powerful (UMP) test exists and a generalized likelihood-ratio test (GLRT) is the standard approach (Kay (1998)).

We have an idea i.e. model of the impact of fault ($\mathbf{M}$) and we try to estimate θ assuming H_1. $\hat{\theta}$ is the maximum likelihood estimator of θ under H_1,

$$\hat{\theta} = (\mathbf{M}^T\mathbf{M})^{-1}\mathbf{M}^T \ {}^n\tilde{\boldsymbol{\gamma}}^f_{1:N}, \tag{13}$$

which is correlated against ${}^n\tilde{\boldsymbol{\gamma}}^f_{1:N}$ to see whether the H_1 we assumed is true or not. Using GLRT we derive (Appendix B) the test statistic ${}^nq^f_N$ for each n^{th} satellite and decide H_1 if,

$${}^nq^f_N = ({}^n\tilde{\boldsymbol{\gamma}}^f_{1:N})^T\mathbf{M}\hat{\theta} > T_N, \tag{14}$$

where T_N is the threshold.

The estimator-correlator test statistic can be simplified as

$${}^nq^f_N = \mathbf{M}^T\mathbf{M}\hat{\theta}^2. \tag{15}$$

Under fault-free conditions the test statistic is central Chi-squared distributed with a single degree of freedom

$${}^nq_N \sim \chi^2_1. \tag{16}$$

The threshold T_N can thus be determined from inverse CDF of Chi-square distribution given the false alarm requirement.

For fault with actual θ magnitude, the test statistic (${}^nq^f_N$) is non-central Chi-squared $\chi^2_1(\lambda)$ distributed with non-centrality parameter

$$\lambda = \mathbf{M}^T\mathbf{M}\theta^2. \tag{17}$$

The missed detection probability for this detector is

$$P_{MD}(M,\theta,N) = 1 - Q\left(Q^{-1}\left(\frac{P_{FA}}{2}\right) - \sqrt{\lambda}\right) + Q\left(Q^{-1}\left(\frac{P_{FA}}{2}\right) + \sqrt{\lambda}\right), \tag{18}$$

where Q is the Q-function of standard normal distribution, and P_{FA} is the probability of false alarm requirement for each satellite. Given the P_{MD} requirement, we can determine the minimum window length N_{min} to ensure the detection of any magnitude larger than θ.

III. RESULTS

We evaluate the performance of the monitor for an example scenario where an aircraft is cruising at level flight using GPS constellation and a navigation grade IMU (specifications in appendix C). Single frequency GPS code and carrier phase measurements with a measurement frequency of 2 Hz is utilized. A total of 6 satellites are in view with a ramp fault of magnitude 4 cm/s occurring in satellite vehicle (SV) 1. Monitor false alarm allocation is 10^{-5} per satellite. Figure 2 illustrates the detection result for this example scenario. The faulted SV 1 can be seen to have increasing test statistic over time with detection being triggered just over a minute. The test statistic growth mimics the deterministic effect of the ramp fault with additive noise.

There are several factors that contribute to satellite fault detection in a KF architecture. First, the IMU dynamic model plays a role in fault detection since it provides measurements that are transformed into range domain to be compared directly to satellite measurements. The higher the grade on IMU the faster the detection of satellite faults. Second, once the innovations are

transformed into the position domain, redundant satellites contribute to the detection of faulty satellites. Third, the higher the number of fault-free satellites, the faster the detection of faults. Lastly, the GNSS error model dynamics such as cycle integer ambiguity and clock bias error models also contribute to the detection of satellite faults.

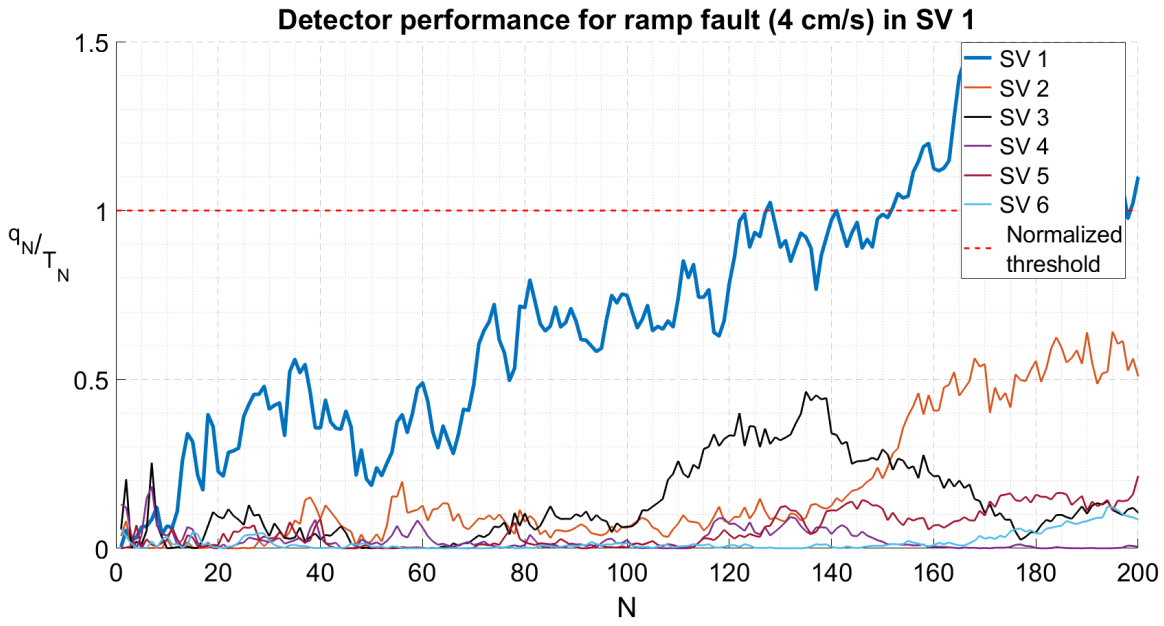

Figure 2: *Example detector performance for satellite ramp fault (4 cm/s) on SV 1.*

IV. IDENTIFICATION AND EXCLUSION

Once detection occurs, we need to identify the faulty satellite and exclude it from the KF. A faulty satellite will typically trigger its channel test statistic but due to the recursive nature of KF, the fault on one satellite might trigger test statistic of other satellite channels as well. This makes the identification and exclusion of faulty satellites difficult. We propose an identification and exclusion algorithm that also does not require a bank of parallel KF. Figure 3 illustrates the process of faulty satellite identification and exclusion.

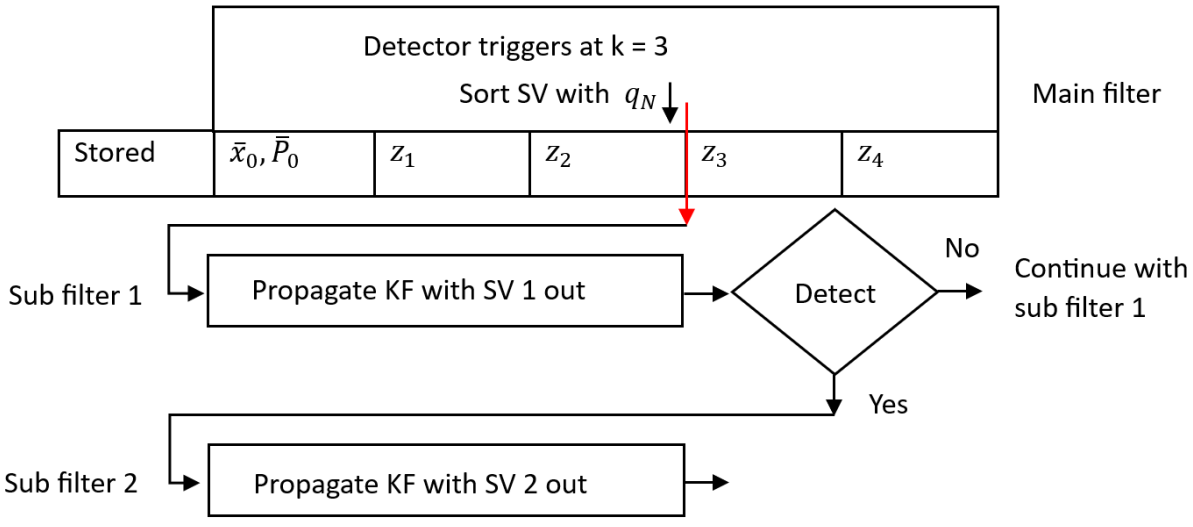

Figure 3: *Illustration of identification and exclusion algorithm.*

First, at the start of every detection window, we propose to store initial conditions (such as $\bar{\mathbf{x}}_\mathbf{0}$ and $\bar{\mathbf{P}}_\mathbf{0}$). If the previous detection window did not trigger a fault, we can say that the probability of fault not being detected at the start of the current window is P_{MD}. As we march forward in time, we also store the GNSS and IMU measurements ($\mathbf{z}_0, \mathbf{z}_1, \mathbf{z}_2, ..$). This is the main filter with all the satellites. Second, once detection is triggered, we sort the test statistic in descending order. The reasoning for this is that the faulty satellite will typically be the one with the largest test statistic. Third, we exclude the satellite with the largest test statistic from the time that we started the current detection window. Using the fault-free initial conditions and the stored measurements, we propagate the sub-filter which excludes the satellite with the largest test statistic. Fourth, we let the monitor detect any faults inside this sub-filter and if we do not trigger any detection, it is confirmed that the excluded satellite was faulty, and we continue our navigation with the sub-filter. Fifth, if the monitor triggers, it means that the faulty satellite is still within the set of this sub-filter. We then exclude the satellite with the next largest test statistic and re-propagate another sub-filter with the remaining satellites. This process continues until we can find a sub- filter that does not trigger any detection. This algorithm allows us to only utilize the available computation power only when a fault detection is triggered, unlike solution separation which always requires running a bank of parallel KF.

V. SEQUENTIAL WINDOWS AND PROTECTION LEVEL

The minimum run length N_{min} for the monitor is determined by Equation (18) and sets the upper limit on the monitor time window. Equation (18) is valid only if fault onset and monitor start time are the same. To capture the fault onset at the start of the detection window, the monitor system is implemented using consecutive fixed-length windows of length N_{min} (Figure 4) with the monitor initialized at the beginning of each window and terminating at the end of each window. A new monitor window is opened at each new GNSS measurement epoch and closed N_{min} epochs later. Figure 4 illustrates the idea, showing (conceptual) PL. At any given instance of time, there will be a set number of monitor windows running, the false alert requirement allocation for each monitor can be equally divided among these monitor windows to determine the thresholds for each. This approach is conservative since the test statistic for the different monitors will be correlated, but it is easy to implement.

We propose the INS-only coasting solution for determining the protection level. Given that the detection window is limited by N_{min}, we can compute the length of time for a protection level originating from an INS-only coasting solution. The INS-only coasting solution drifts over time and thus the window length N_{min} helps to terminate the protection level before it gets unbounded. Thus, this sequence of detection windows with INS-only coasting provides a continuous bounded protection level throughout the exposure time. For even centimeter-level ramp faults, the detection window length does not exceed a few minutes, thus ensuring that the protection level drift does not go unbounded in such a way that typical alert limit requirements are triggered.

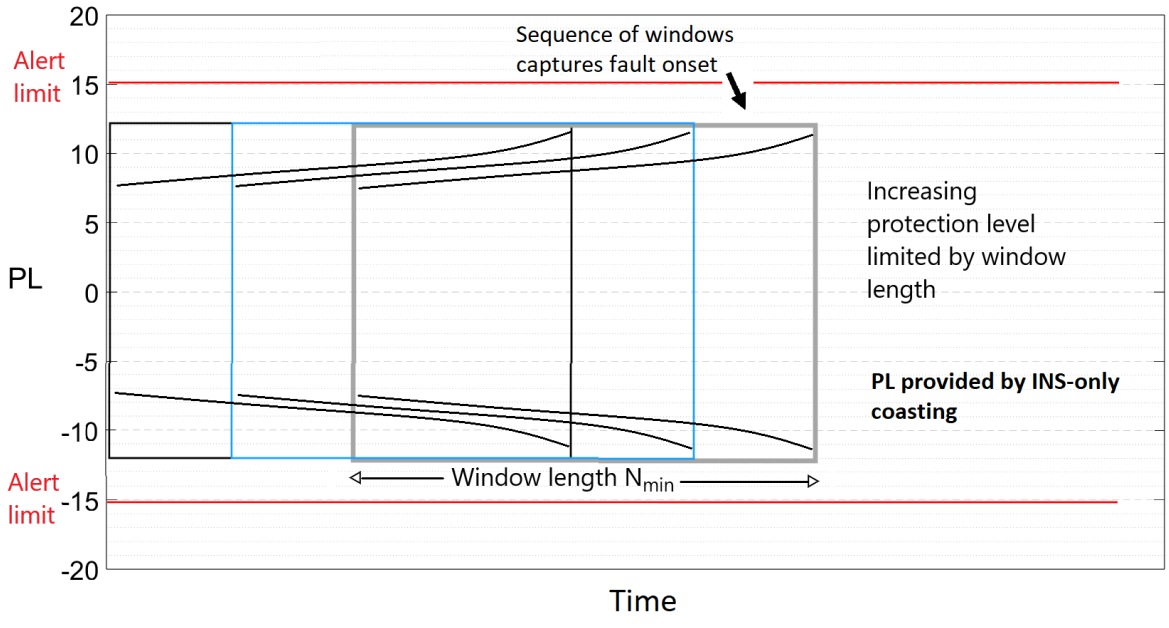

Figure 4: *Illustration of sequential monitor windows with increasing protection levels.*

VI. CONCLUSION

We proposed a satellite channel detector that leverages prior fault mode information. The detector was optimized to the threat space constrained by fault mode and utilized satellite channel-specific sufficient test statistic to detect faults. We quantified the minimum length of the detection window which would ensure the detection of faults larger than a specific magnitude. We also proposed a satellite identification and exclusion algorithm which no longer requires a bank of parallel KF. A sequence of detection windows ensures satellite fault onset capture. Lastly, we propose a protection level using INS-only coasting which is drift-limited by detection window length N_{min}.

A revised test statistic derivation without the linear approximation of fault impact will be presented in details in a future work. We also aim to generalize the fault mode with a polynomial profile which would encompass a larger threat space and allow generalization of the detector. We will evaluate the parametric performance of this detector against different fault profiles and detection window lengths to obtain missed detection bounds for a given threat space.

REFERENCES

Angus, J. E. (2006). RAIM with multiple faults. *NAVIGATION: Journal of the Institute of Navigation*, 53(4):249–257. https://doi.org/10.1002/j.2161-4296.2006.tb00387.x.

Blanch, J., Walker, T., Enge, P., Lee, Y., Pervan, B., Rippl, M., Spletter, A., and Kropp, V. (2015). Baseline advanced raim user algorithm and possible improvements. *IEEE Transactions on Aerospace and Electronic Systems*, 51(1):713–732. https://doi.org/10.1109/TAES.2014.130739.

Brenner, M. (1996). lntegrated GPS/inertial fault detection availability. *NAVIGATION*, 43(2):111–130. https://doi.org/10.1002/j.2161-4296.1996.tb01920.x.

DO-384 (2020). Minimum operational oerformance standards (MOPS) for GNSS aided inertial systems. Standard, SC 159, Radio Technical Commission for Aeronautics (RTCA). https://standards.globalspec.com/std/14369517/RTCADO-384.

Joerger, M. and Pervan, B. (2013). Kalman filter-based integrity monitoring against sensor faults. *AIAA Journal of Guidance, Control and Dynamics*, 36(2):349–361. https://doi.org/10.2514/1.59480.

Kay, M. S. (1998). *Fundamentals of Statistical Signal Processing: Detection Theory, Volume 2*. Prentice-Hall PTR.

Knowles, D. and Gao, G. (2023). Euclidean distance matrix-based rapid fault detection and exclusion. *NAVIGATION: Journal of the Institute of Navigation*, 70(1). https://doi.org/10.33012/navi.555.

Parkinson, B. W. and Axelrad, P. (1988). Autonomous gps integrity monitoring using the pseudorange residual. *NAVIGATION*, 35(2):255–274. https://doi.org/10.1002/j.2161-4296.1988.tb00955.x.

Quartararo, J. D. and Langel, S. E. (2022). Detecting slowly accumulating faults using a bank of cumulative innovations monitors in kalman filters. *NAVIGATION: Journal of the Institute of Navigation*, 69(1). https://doi.org/10.33012/navi.507.

Tanil, C., Khanafseh, S., Joerger, M., and Pervan, B. (2018). Sequential integrity monitoring for kalman filter innovations-based detectors. In *Proceedings of the 31st International Technical Meeting of The Satellite Division of The Institute of Navigation (ION GNSS+ 2018)*, pages 2440–2455. https://doi.org/10.33012/2018.15975.

Wendel, J. (2022). GNSS pseudorange fault detection and exclusion with multiple outliers. In *Proceedings of the 35th International Technical Meeting of The Satellite Division of The Institute of Navigation (ION GNSS+ 2022)*, pages 1481–1495. https://doi.org/10.33012/2022.18421.

APPENDIX

A. Cumulative effect of prior faults on innovations

We start with fault starting time as $k = 1$, and will denote presence of fault with superscript f. The faulty measurement $\mathbf{z}_1^f$ at $k = 1$ is

$$\mathbf{z}_1^f = \mathbf{z}_1 + \bar{\mathbf{f}}_1 \tag{19}$$

where $\mathbf{z}_1$ is the fault-free measurement, and $\bar{\mathbf{f}}_1$ is the fault vector at time $k = 1$.

The faulted innovations at time $k = 1$ is

$$\gamma_1^f = \gamma_1 + \bar{\mathbf{f}}_1 \tag{20}$$

where γ_1 is the fault-free innovation.

Now, for time $k = 2$, the faulted innovation vector is

$$\gamma_2^f = \gamma_2 + \bar{\mathbf{f}}_2 - \mathbf{H}_2\mathbf{\Phi}_2[\mathbf{K}_1\bar{\mathbf{f}}_1] \tag{21}$$

We introduce three new variables here, Ω, β, and $\mathbf{b}$, which are defined for $k > 1$ as

$$\mathbf{\Omega}_{k-1} = \mathbf{\Phi}_{k-1}[\mathbf{\Omega}_{k-2} + \mathbf{K}_{k-2}\boldsymbol{\beta}_{k-2}] \tag{22}$$

$$\boldsymbol{\beta}_{k-1} = \bar{\mathbf{f}}_{k-1} - \mathbf{H}_{k-1}\mathbf{\Omega}_{k-1} \tag{23}$$

$$\mathbf{b}_k = -\mathbf{H}_k\mathbf{\Phi}_k[\mathbf{\Omega}_{k-1} + \mathbf{K}_{k-1}\boldsymbol{\beta}_{k-1}] \tag{24}$$

and zero for $k \leq 1$.

For $k = 2$

$$\mathbf{\Omega}_1 = \mathbf{\Phi}_1[\mathbf{\Omega}_0 + \mathbf{K}_0\boldsymbol{\beta}_0] = 0 \tag{25}$$

$$\boldsymbol{\beta}_1 = \bar{\mathbf{f}}_1 - \mathbf{H}_1\mathbf{\Omega}_1 = \bar{\mathbf{f}}_1 \tag{26}$$

and

$$\mathbf{b}_2 = -\mathbf{H}_2\mathbf{\Phi}_2[\mathbf{\Omega}_1 + \mathbf{K}_1\boldsymbol{\beta}_1] \tag{27}$$

Substituting Equation (25) and (26)in Equation (21) we rewrite

$$\gamma_2^f = \gamma_2 + \bar{\mathbf{f}}_2 - \mathbf{H}_2\mathbf{\Phi}_2[\mathbf{\Omega}_1 + \mathbf{K}_1\boldsymbol{\beta}_1] \tag{28}$$

Again, substituting Equation (27) in Equation (28)

$$\gamma_2^f = \gamma_2 + \bar{\mathbf{f}}_2 + \mathbf{b}_2 \tag{29}$$

Now the expression for faulted innovation vector for time $k = 3$ is

$$\gamma_3^f = \gamma_3 + \bar{\mathbf{f}}_3 - \mathbf{H}_3\mathbf{\Phi}_3[\mathbf{\Phi}_2\mathbf{K}_1\bar{\mathbf{f}}_1 + \mathbf{K}_2[\bar{\mathbf{f}}_2 - \mathbf{H}_2\mathbf{\Phi}_2[\mathbf{K}_1\bar{\mathbf{f}}_1]]] \tag{30}$$

Again for $k = 3$

$$\mathbf{\Omega}_2 = \mathbf{\Phi}_2[\mathbf{\Omega}_1 + \mathbf{K}_1\boldsymbol{\beta}_1] \tag{31}$$

$$\boldsymbol{\beta}_2 = \bar{\mathbf{f}}_2 - \mathbf{H}_2\mathbf{\Omega}_2 \tag{32}$$

and

$$\mathbf{b}_3 = -\mathbf{H}_3\mathbf{\Phi}_3[\mathbf{\Omega}_2 + \mathbf{K}_2\boldsymbol{\beta}_2] \tag{33}$$

Substituting Equations (25) and (26) in (31) we rewrite,

$$\mathbf{\Omega}_2 = \mathbf{\Phi}_2[\mathbf{K}_1\bar{\mathbf{f}}_1] \tag{34}$$

Substituting Equations (34) in (30)

$$\gamma_3^f = \gamma_3 + \bar{\mathbf{f}}_3 - \mathbf{H}_3\mathbf{\Phi}_3[\mathbf{\Omega}_2 + \mathbf{K}_2[\bar{\mathbf{f}}_2 - \mathbf{H}_2\mathbf{\Omega}_2]] \tag{35}$$

Now substituting Equation (32) in (35)

$$\gamma_3^f = \gamma_3 + \bar{\mathbf{f}}_3 - \mathbf{H}_3\mathbf{\Phi}_3[\mathbf{\Omega}_2 + \mathbf{K}_2\boldsymbol{\beta}_2] \tag{36}$$

Finally, substituting Equation (33) in (36)

$$\gamma_3^f = \gamma_3 + \bar{\mathbf{f}}_3 + \mathbf{b}_3 \tag{37}$$

Thus, in general we can write,

$$\gamma_k^f = \gamma_k + \bar{\mathbf{f}}_k + \mathbf{b}_k \tag{38}$$

where $\mathbf{b}_k$ is the cumulative effect of prior faults on current innovation vector and is given by Equation (24).

B. Derivation of test statistic for detection of deterministic fault with unknown amplitude

The normalized innovations vector from Equation (11) for exposure time N with the deterministic impact ($\mathbf{D}_{1:N}$) of fault on n^{th} satellite is

$$ {}^{n}\tilde{\boldsymbol{\gamma}}^{f}_{1:N} = \mathbf{D}_{1:N} + {}^{n}\tilde{\boldsymbol{\gamma}}_{1:N} \tag{39} $$

Using the approximation

$$ \mathbf{D}_{1:N} \approx \mathbf{M}\theta = [1 \quad 2 \quad 3 \quad . \quad . \quad . \quad N]^{T}\theta \tag{40} $$

where θ is the unknown amplitude of fault impact,

$$ {}^{n}\tilde{\boldsymbol{\gamma}}^{f}_{1:N} = \mathbf{M}\theta + {}^{n}\tilde{\boldsymbol{\gamma}}_{1:N} \tag{41} $$

with, null hypothesis $H_0 : \theta = 0$, and alternative hypothesis $H_1 : \theta \neq 0$. Using generalized likelihood ratio test (GLRT), given two mutually exclusive hypotheses H_0 and H_1, which for some observation ${}^{n}\tilde{\boldsymbol{\gamma}}_{1:N}$ have conditional probability densities $p_0({}^{n}\tilde{\boldsymbol{\gamma}}_{1:N}|H_0)$ and $p_1({}^{n}\tilde{\boldsymbol{\gamma}}_{1:N}|\hat{\theta}, H_1)$, the likelihood ratio given an arbitrary threshold $T(N)$ is

$$ \Lambda({}^{n}\tilde{\boldsymbol{\gamma}}_{1:N}) = \frac{p_1({}^{n}\tilde{\boldsymbol{\gamma}}_{1:N}|\hat{\theta}, H_1)}{p_0({}^{n}\tilde{\boldsymbol{\gamma}}_{1:N}|H_0)} \underset{H_0}{\overset{H_1}{\gtrless}} T(N) \tag{42} $$

where $\hat{\theta}$ is the maximum likelihood estimate of θ under H_1 (Kay (1998))

$$ \hat{\theta} = \frac{\sum_{k=1}^{N} {}^{n}\tilde{\boldsymbol{\gamma}}_{k}\mathbf{M}_{k}}{\sum_{k=1}^{N}\mathbf{M}_{k}^{2}} \tag{43} $$

Expanding Equation (42)

$$ \Lambda({}^{n}\tilde{\boldsymbol{\gamma}}_{1:N}) = \frac{\frac{1}{(2\pi\,{}^{n}\sigma)^{\frac{N}{2}}}\exp\left(-\frac{1}{2\,{}^{n}\sigma^{2}}\sum_{k=1}^{N}({}^{n}\tilde{\boldsymbol{\gamma}}_{k} - \mathbf{M}_{k}\hat{\theta})^{2}\right)}{\frac{1}{(2\pi\,{}^{n}\sigma)^{\frac{N}{2}}}\exp\left(-\frac{1}{2\,{}^{n}\sigma^{2}}\sum_{k=1}^{N}{}^{n}\tilde{\boldsymbol{\gamma}}_{k}{}^{2}\right)} \underset{H_0}{\overset{H_1}{\gtrless}} T(N), \tag{44} $$

where ${}^{n}\sigma^{2}$ is the variance of normalized innovation for n^{th} channel. Substituting ${}^{n}\sigma^{2} = 1$, the above equation simplifies to

$$ \Lambda({}^{n}\tilde{\boldsymbol{\gamma}}_{1:N}) = \frac{\exp\left(-\frac{1}{2}\sum_{k=1}^{N}({}^{n}\tilde{\boldsymbol{\gamma}}_{k} - \mathbf{M}_{k}\hat{\theta})^{2}\right)}{\exp\left(-\frac{1}{2}\sum_{k=1}^{N}{}^{n}\tilde{\boldsymbol{\gamma}}_{k}{}^{2}\right)} \underset{H_0}{\overset{H_1}{\gtrless}} T(N), \tag{45} $$

Taking log on both sides we obtain

$$ -\frac{1}{2}\sum_{k=1}^{N}\left(-2\hat{\theta}\mathbf{M}_{k}{}^{n}\tilde{\boldsymbol{\gamma}}_{k} + \hat{\theta}^{2}\mathbf{M}_{k}^{2}\right) \underset{H_0}{\overset{H_1}{\gtrless}} \ln T(N), \tag{46} $$

Using Equation (43) for $\hat{\theta}$ in Equation (46) above and simplifying

$$ -\frac{1}{2}\left(-2\hat{\theta}\hat{\theta}\sum_{k=1}^{N}\mathbf{M}_{k}^{2} + \hat{\theta}^{2}\sum_{k=1}^{N}\mathbf{M}_{k}^{2}\right) \underset{H_0}{\overset{H_1}{\gtrless}} \ln T(N), \tag{47} $$

Simplifying the above equation

$$ \hat{\theta}^{2}\left(\sum_{k=1}^{N}2\mathbf{M}_{k}^{2} - \mathbf{M}_{k}^{2}\right) \underset{H_0}{\overset{H_1}{\gtrless}} 2\ln T(N), \tag{48} $$

Simplifying further

$$ \hat{\theta}^{2}\left(\sum_{k=1}^{N}\mathbf{M}_{k}^{2}\right) \underset{H_0}{\overset{H_1}{\gtrless}} 2\ln T(N), \tag{49} $$

Equation (49) can be equivalently written as defining our test statistic

$$ {}^{n}q_{N}^{f} = \mathbf{M}^{T}\mathbf{M}\hat{\theta}^{2} \underset{H_0}{\overset{H_1}{\gtrless}} 2\ln T(N) \tag{50} $$

C. Sensor specifications

Table 2: Navigation grade IMU specifications

Parameter	Value	Units
Velocity random walk	1.43×10^{-2}	m/s/$\sqrt{\text{h}}$
Accelerometer bias instability	1×10^{-2}	mg
Accelerometer bias repeatability	2.5×10^{-2}	mg
Accelerometer bias time constant	3600	s
Angular random walk	1×10^{-3}	deg/$\sqrt{\text{h}}$
Gyroscope bias instability	3.5×10^{-3}	deg/h
Gyroscope bias repeatability	3×10^{-3}	deg/h
Gyroscope time constant	3600	s